α-cluster structure above double closed shells

T. T. Ibrahim,[1] A. C. Merchant,[2] S. M. Perez,[3,4,*] and B. Buck[2]

[1]*Department of Physics, Federal University Lokoja, PMB 1154, Lokoja, Nigeria*

[2]*Department of Physics, University of Oxford, Theoretical Physics, Beecroft Building, Parks Road, Oxford OX1 3PU, United Kingdom*

[3]*Department of Physics, University of Cape Town, Private Bag, Rondebosch 7700, South Africa*

[4]*iThemba LABS, PO Box 722 Somerset West 7129, South Africa*

(Received 27 April 2019; published 28 June 2019)

Spectra, reduced electromagnetic $B(E2)$ transition strengths, mean-square charge radii and, for those states above the emission threshold, α-decay widths are calculated by using a local potential cluster model for the ground state $K^\pi = 0^+$ and first-excited $K^\pi = 0^-$ bands of ^{20}Ne, ^{44}Ti, ^{94}Mo, ^{104}Te, and ^{136}Te. These nuclei are all modeled as α-particles outside double-closed-shell core. The nuclear cluster-core potential is taken as a mixture of Saxon-Woods and cubed Saxon-Woods terms whose depths, radii, and diffuseness parameters are determined by the double folding Michigan-3-Yukawa potential model. Generally good agreement with experimental data is obtained without the introduction of effective charges, and predictions are made for many as yet unmeasured quantities in the two Te isotopes.

DOI: 10.1103/PhysRevC.99.064332

I. INTRODUCTION

Many nuclear structure models have been put forward to describe the complex and ever-increasing experimental nuclear data from the fundamental investigations of nucleonic behavior and excitations. The widely accepted and successful shell-model techniques, however, even with present-day computational power, cannot handle a sufficiently large basis to adequately account for the clustering correlation and its experimental signatures; namely, the spatial localization of clusters evidenced by the observed inversion doublets, large cluster decay width, selective excitations of the cluster states, and the electric monopole transitions between the excited 0^+ state and the ground state of some light nuclei [1–7]. The shortcomings of the existing sophisticated mean-field models, largely due to computational limitations, contributes to the continued interest in the development of the nuclear cluster models in addition to shell-model techniques, so that the two approaches complement one another. The nonlocal resonating group method (RGM), the generator coordinate method (GCM), and the antisymmetrized molecular dynamics (AMD) are some of the microscopic cluster models that fully consider the nucleon antisymmetrization between the clusters. More recently, a shell-model technique has been advanced to obtain clustering spectroscopic information from the overlap of large shell-model configurations in a harmonic-oscillator basis [8]. These models are found successfully to describe the clustering properties of light nuclei. They are, however, characterized by attendant computational difficulties when extending them to heavy nuclei.

The local potential cluster model, a simplified form of the RGM technique [2,9], has been used by several authors to describe the properties of light and heavy nuclei. The model treats a nucleus as a two-cluster system interacting through a deep local potential. The intercluster interaction is assumed to be weak compared with the interactions within the clusters so that the relative motion between the clusters becomes the dominant nuclear motion of the nucleus. Central to the model is therefore the choice of the local interaction which can be used to describe the bound and quasibound state properties of the parent nucleus and can also serve as the real component of the optical potential to describe the scattering properties of the clusters [10,11]. The interaction may either be a phenomenological potential with free parameters or nuclear densities folded with effective nucleon-nucleon (NN) interactions depending on the degree of simplification with respect to the fundamental NN interaction. With an appropriate interaction the model naturally generates the ground and excited bands (and from the associated wave functions their respective properties) of a nucleus. We previously used a local interaction which combines the best features of a Saxon-Woods form and a microscopic Michigan-3-Yukawa (M3Y) interaction to investigate the properties of heavy nuclei [12,13]. A natural extension of our earlier works is to investigate the light nuclei with well-established α-cluster structure. In the present work, motivated by recent experimental measurements [14–16], the properties of the α-cluster states in ^{20}Ne, ^{44}Ti, ^{94}Mo, and ^{104,136}Te are studied by using the improved hybrid potential derived from the M3Y interaction. These nuclei, each described as an α-particle–double-closed-shell-core system, provide excellent fertile ground for systematic investigation of nuclear α-clustering in light- and medium-mass nuclei. The observation of the predicted $K^\pi = 0^-$ negative-parity partner of the $K^\pi = 0^+$ ground band in ^{44}Ti is indicative of the

*Deceased.

successes of the local potential approach and of the α-cluster structure of that nucleus [15,17–22]. It is expected that similar partner bands will exist in heavier nuclei with the α-particle–double-closed-shell-core structure. The investigation of the negative-parity bands, especially in ^{94}Mo and ^{136}Te, that are yet to be measured is of considerable interest.

The previously used (SW + SW^3) model has consistently generated an underbound 0^+ ground state which was attributed to the internal structure of the potential model [23]. Recently we considered an additional interaction which was chosen to account for the possible overlap between the core-cluster system. The overlap was found to be more pronounced in the α-cluster structure of ^{212}Po compared with that inferred for the exotic cluster structure of heavier actinide nuclei. It would be interesting to determine whether similar findings also hold for the lighter α-particle–double-closed-shell-core systems.

II. MODEL FORMALISM

The physically appealing and intuitive local potential model treats a nucleus as a spatially separated unexcited core and α-cluster system such that the properties of the nucleus are given by the Schrödinger wave equation

$$\left(-\frac{\hbar^2}{2\mu}\nabla^2 + V(r)\right)|n,l,m\rangle = E_{nl}|n,l,m\rangle, \tag{1}$$

which describes their relative motion. The potential $V(r)$ describes the interaction between the α-particle and the core nuclei in a single channel. It is taken as the sum of the strong nuclear and Coulomb interactions. The bound and quasibound state wave functions $|n,l,m\rangle$ and the associated energies E_{nl} are then taken to describe the α-cluster states of the parent nucleus. Clearly, at the heart of the problem is the interaction $V(r)$ which needs to be appropriately defined. Following our earlier works [12,13], we take the nuclear interaction as a Saxon-Woods (SW + SW^3) function of the form

$$V_N(r,R) = -V_o\left[\frac{x}{1+\exp\left(\frac{r-R}{a}\right)} + \frac{1-x}{\left[1+\exp\left(\frac{r-R}{3a}\right)\right]^3}\right], \tag{2}$$

which has been successfully used to describe the alpha and exotic cluster states in heavy nuclei [10,24,25]. Values of the strength V_o, the radius R, the diffuseness a, and the mixing parameter x are determined by using the double-folding Michigan-3-Yukawa potential model,

$$V_N(\boldsymbol{r}) = \lambda \iint \rho_c(\boldsymbol{r_1})\rho_\alpha(\boldsymbol{r_2})[v(\boldsymbol{r}_{12}) + \hat{J}_{00}(E')\delta(\boldsymbol{r}_{12})]d\boldsymbol{r_1}d\boldsymbol{r_2}, \tag{3}$$

where λ is the renormalization factor, $\rho_c(\boldsymbol{r_1})$ and $\rho_\alpha(\boldsymbol{r_2})$ are the core and the alpha-particle nuclear densities. The nucleon-nucleon (NN) interaction $v(\boldsymbol{r}_{12})$ is taken as the effective density-independent M3Y interaction:

$$v(r_{12}) = 7999\frac{\exp(-4r_{12})}{4r_{12}} - 2134\frac{\exp(-2.5r_{12})}{2.5r_{12}}, \tag{4}$$

and the zero-range pseudopotential

$$\hat{J}_{00}(E')\delta(\boldsymbol{r}_{12}) = -276(1 - 0.005E'/A_2)\delta(r_{12}), \tag{5}$$

accounts for the exchange interaction. The energy E' is given by the α-particle–core threshold energy, and A_2 is the mass number of the α-cluster.

We take the Coulomb interaction as that of a point cluster interacting with a uniformly charged spherical core,

$$\begin{aligned} V_C(r) &= \frac{Z_1Z_2e^2}{r} && \text{if } r \geqslant R_C \\ &= \frac{Z_1Z_2e^2}{2R_C}\left(3 - \left|\frac{r}{R_C}\right|^2\right) && \text{if } r \leqslant R_C, \end{aligned} \tag{6}$$

with quantities Z_1 and Z_2 being the charge numbers of the core and the α-cluster, and where the Coulomb radius R_C is assumed to be equal to the nuclear radius R to minimize the number of free model parameters.

The parameters of the interaction in Eq. (2) are determined following the procedure outlined in Ref. [13] with the best parameter set determined by using the mean-square energy deviation as the goodness-of-fit criterion:

$$\mathcal{S}^2 = \frac{\sum_l \left(E_{nl}^{\text{expt}} - E_{nl}^{\text{calc}}\right)^2}{N}, \tag{7}$$

where N is the number of cluster-state energies used in the minimization procedure. We used the Wildermuth rule $G = \sum_{i=1}(2n_i + l_i) - \bar{g}$ to ensure that the nucleons of the core and of the cluster do not occupy the same states. The quantum numbers n_i and l_i are simply the number of interior nodes of the radial wave function and the orbital angular momentum of the cluster nucleons, while $\bar{g}$ is the number of quanta taken up by the cluster internal motion. This condition (and of course the calculation of the cluster-state energies) can easily be implemented by using the Bohr-Sommerfeld integral [10,12,24,25].

The nuclear electromagnetic properties are generally known to provide stringent tests of nuclear model predictions due to their dependence on the state wave functions. For this purpose the α-core relative motion wave functions are used to evaluate the in-band reduced quadrupole transition ($\ell = 2$) probabilities whose general form is

$$B(E\ell; l_i \longrightarrow l_f) = \left(\frac{\hat{l}_f}{\hat{l}_i}\right)^2 |\langle n, l_f||\beta_\ell r^\ell Y_\ell||n, l_i\rangle|^2, \tag{8}$$

where $\hat{l}$ is $\sqrt{2l+1}$, Y_ℓ is a spherical harmonic with multipole ℓ, and the factor β_ℓ is given by

$$\beta_\ell = \left[Z_1\left(\frac{-A_2}{A}\right)^\ell + Z_2\left(\frac{A_1}{A}\right)^\ell\right], \tag{9}$$

with A_1 and A_2 being the core and the α-cluster mass numbers, respectively.

The degree of clustering and the possible overlap of a core-cluster system may also be deduced from the mean-square cluster-core separation

$$\langle r^2\rangle = \int_0^\infty \psi_L^*(r)r^2\psi_L(r)dr, \tag{10}$$

TABLE I. The best-fit parameter values of the (SW + SW^3) interaction for the α-core system of ^{20}Ne, ^{44}Ti, ^{94}Mo, and ^{136}Te nuclei.

Nucleus	V_o (MeV)	R (fm)	a (fm)	x	G	$\mathcal{S}^2$
^{20}Ne	242.30	3.094	0.688	0.31	8	2.77×10^{-1}
^{44}Ti	235.09	3.960	0.770	0.51	12	4.19×10^{-1}
^{94}Mo	240.98	5.230	0.759	0.46	16	5.81×10^{-2}
^{136}Te	244.98	5.822	0.751	0.43	18	1.54×10^{-2}

and the charge radius

$$\langle R^2\rangle = \frac{1}{Z}[Z_1\langle r^2\rangle_c + Z_2\langle r^2\rangle_\alpha + \beta_2\langle r^2\rangle], \tag{11}$$

of the parent nucleus. Here $\langle r^2\rangle_c$ and $\langle r^2\rangle_\alpha$ are the mean-square charge radii of the core and the α-cluster, respectively.

III. RESULTS AND DISCUSSION

A. Potential parameters

For our purpose the density distributions are taken from the experimental parametrization of elastic-scattering data [26]. The three-parameter Fermi (3pF) function

$$\rho_c(r_1) = \frac{\rho_o\left(1 + wr_1^2/c^2\right)}{1 + \exp\left(\frac{r_1 - c}{a}\right)}, \tag{12}$$

with $w = -0.051$, $c = 2.608$ fm, and $a = 0.513$ fm, is used for the ^{16}O core and, $w = -0.161$, $c = 3.766$ fm, and $a = 0.586$ fm are used for the ^{40}Ca core nucleus. Similarly, the three-parameter Gaussian (3pG) model

$$\rho_c(r_1) = \frac{\rho_o\left(1 + wr_1^2/c^2\right)}{1 + \exp\left(\frac{r_1^2 - c^2}{a^2}\right)}, \tag{13}$$

with $w = -0.350$, $c = 4.434$ fm, and $a = 2.528$ fm is taken for ^{90}Zr. However, due to the unavailability of similar experimental data for ^{132}Sn, we use the general two-parameter Fermi model,

$$\rho_c(r_1) = \frac{\rho_o}{1 + \exp\left(\frac{r_1 - c}{a}\right)}, \tag{14}$$

whose radius is taken to be $c = 1.07A_1^{1/3}$ and the diffuseness $a = 0.54$ fm. For each of the density distributions, the central density ρ_o is obtained by normalizing the densities to the respective mass numbers A_1 of the core nuclei. The Gaussian density distribution

$$\rho_\alpha(r_2) = 0.4299\exp\left(-0.7024r_2^2\right) \tag{15}$$

is used for the α-cluster density $\rho_\alpha(r_2)$.

The hybrid potential parameters obtained from fits to the surface part of the M3Y interaction are presented in Table I with their respective optimization parameters $\mathcal{S}^2$. The potential depths are seen to scale approximately as $V_o \sim 60A_2$ MeV. The range of values deduced for the reduced radius $r_o =$ 1.12–1.15 fm is consistent with the widely accepted range $r_o =$ 1.10–1.25 fm, but tighter.

B. α-cluster states

The α-cluster states of light nuclei are mostly populated by using resonance alpha-particle scattering, alpha-transfer reactions such as the $(^6\text{Li}, d)$ reaction as well as the angle correlation $(^7\text{Li}, t\alpha)$ reactions for highly excited cluster states [4,15,20,21]. The states are generally known to be characterized by a relatively large α-decay width and enhanced electromagnetic $B(E2)$ transition probabilities. The quasirotational nature of the yrast bands in these nuclei is well established.

I. ^{20}Ne

Several experimental efforts have reconfirmed the aforementioned properties with improved data, especially for the most easily accessible ^{20}Ne and ^{44}Ti nuclear cluster states [14,15,21]. For ^{20}Ne the decay threshold is 4.729 MeV with the lowest 0^+, 2^+, and 4^+ states bound against α decay. The 6^+ and 8^+ of the ground band, together with the lowest excited negative-parity band, are quasibound with significant α-decay width. The ground-state band is characterized with appreciable measured quadrupole transition strengths. Their decay widths and transition strengths are, however, found to be small compared with those of the $K^\pi = 0^-$ negative-parity band with bandhead placed at 5.788 MeV. The single-particle approach and even advanced shell-model techniques cannot explain the observed doublet structure of ^{20}Ne [14]. The cluster model on the other hand provides a natural interpretation of these observed properties. The results of the present calculations for ^{20}Ne are compared with the experimental data in Table II. The energy structure of both the positive- and negative-parity bands is satisfactorily reproduced except for the slight upward shift of the calculated negative-parity band. Our calculation also underbinds the 0^+ head of the ground-state band. This is interpreted as a shortcoming of the interaction in the interior [23]. The order of magnitude and the trend of our calculated transition strengths are consistent with the measured values. The predicted values for the negative-parity band show strongly enhanced $B(E2)$ transition strengths, an order of magnitude larger than those of the positive-parity band. We emphasize here that the $B(E2; l_i \longrightarrow l_f)$ have been calculated without the use of an effective charge as in the shell-model approach. Following Refs. [10,23] we evaluate the complex energy solution of the Schrödinger wave equation using the code GAMOW [27]. The calculated α-decay widths, based on the corresponding experimental excitation energies, are compared with the experimental widths in Table II. The results are also seen to agree with previously predicted values for both the positive- and negative-parity bands [10,23,28]. The mean-square separations deduced for the positive-parity band are seen to decrease with increasing angular momentum. This can be understood from the wave functions in Fig. 1. We see that the surface extension and the peak position at the surface decreases with increasing angular momentum, which is the centrifugal antistretching effect. This phenomenon is also seen in the trend obtained for the negative-parity band in which the value of the mean separation peaks for the 5^- state. This is an interesting instance of the antistretching effect, only setting in halfway up the band, at higher spin. The corresponding wave functions in Fig. 2 show a 5^- state with

TABLE II. The measured and calculated energy levels, the reduced transition strengths $B(E2\downarrow)$, and the α-decay widths Γ_α of ^{20}Ne. The last column indicates the mean-square separation of the α-core system.

	Energy (MeV)		Quadrupole transition (e^2 fm^4)		Decay widths (keV)		Mean-square separation
J^π	$E_{\rm expt}$	$E_{\rm calc}$	$B(E2\downarrow)_{\rm expt}$	$B(E2\downarrow)_{\rm calc}$	$\Gamma_\alpha^{\rm expt}$	$\Gamma_\alpha^{\rm calc}$	$\langle r^2\rangle_{\rm calc}$ (fm^2)
0^+	0.000	(0.357)					15.107
2^+	1.634	1.633	65.5 ± 3.2	46.0			15.008
4^+	4.248	4.184	70.9 ± 6.5	59.6			14.396
6^+	8.776	7.883	64.4 ± 9.7	49.0	0.11 ± 0.02	0.57	13.037
8^+	11.951	12.625	29.1 ± 4.2	25.5	0.035 ± 0.010	0.37	10.969
1^-	5.788	6.777			0.028 ± 0.003	0.034	29.216
3^-	7.156	8.594	164 ± 26	248.2	8.2 ± 0.3	12.7	33.469
5^-	10.262	11.770		409.0	145 ± 40	199	43.297
7^-	15.366	16.037		499.3	110 ± 10	561	36.898
9^-	22.870	21.616		118.1	225 ± 40	590	17.555

a well-extended surface and larger peak radius compared with those of the neighboring 3^- and 7^- states. The cluster-core separations for the 0^+ and 8^+ states are found to be 88% and 75% of the total experimental charge radii, implying a more compact cluster structure for the ground state and an undesirable overlap in the band-terminating 8^+ state [19,29]. The larger mean separations obtained for the negative-parity band, on the other hand, are indicative of a more-well-formed α-cluster structure. We find that the root-mean-square (rms) charge radii are weakly dependent on the angular momentum i.e., nearly constant at a value $\sim$3.0 fm. The calculated ^{20}Ne charge-radius values are determined by using the charge radii of 2.730 ± 0.025 and 1.676 ± 0.008 fm for the ^{16}O core and the α cluster, respectively [26]. Our calculated value for the ^{20}Ne ground-state charge radius $\langle R^2\rangle^{1/2} = 2.990$ fm is to be compared with 2.992 ± 0.008 fm deduced from the three-parameter Fermi model in Ref. [26]. In agreement with earlier works the results for all the observables suggest the existence and possible admixture of more complicated configurations, possibly a two-α-cluster system [6] together with mean-field configurations [28], in addition to the single-α-cluster structure for the ground-state band.

2. ^{44}Ti

The experimental investigations of the α-cluster structure in ^{44}Ti has been fairly successful. The currently accepted data on the ground-state band indicate bound 0^+, 2^+, 4^+, and 6^+ states while the 8^+, 10^+, and 12^+ states are above the α-decay threshold. The debate on the lowest nodal band associated with an α-cluster structure has been put to rest by the experimental observation of the negative-parity partner of the ground-state band [20–22]. The existence of the lowest negative-parity band has recently been reconfirmed and extended to the $J^\pi = 7^-$ state by Fukada *et al.* [15]. However, unlike the positive-parity band in which the electromagnetic strength has been measured, the electromagnetic properties of the negative-parity partner band are yet to be measured. It would therefore be a worthwhile exercise to search for the existence of the remaining negative-parity band members, up to the predicted $J^\pi = 13^-$ state, with a view to measuring their respective lifetimes. On the other hand various theoretical

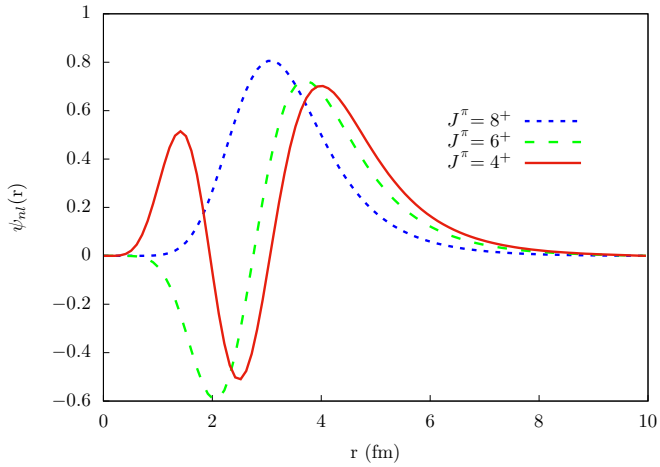

FIG. 1. Relative motion wave functions for the ^{16}O plus α-cluster system with angular momenta $J = 4, 6, 8$ represented by solid, long-dashed, and short-dashed lines, respectively.

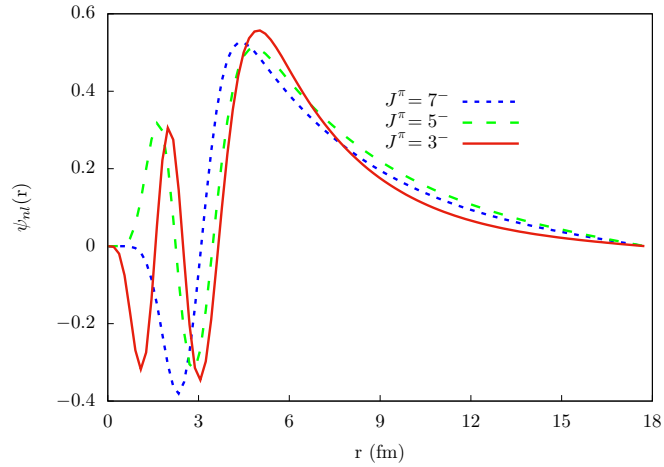

FIG. 2. Same as in Fig. 1 but for angular momenta $J = 3$, 5, 7 represented by solid, long-dashed, and short-dashed lines, respectively.

TABLE III. The measured and calculated energy levels, the reduced transition strengths $B(E2\downarrow)$, and the α-decay widths Γ_α of ^{44}Ti. The last column indicates the mean-square separation of the α-core system. The core charge radius of 3.482 ± 0.025 fm is used. Experimental data are taken from Refs. [15,26,33].

	Energy (MeV)		Quadrupole transition (e^2 fm^4)		Decay widths (keV)		Mean-square separation
J^π	$E_{\rm expt}$	$E_{\rm calc}$	$B(E2\downarrow)_{\rm expt}$	$B(E2\downarrow)_{\rm calc}$	$\Gamma_\alpha^{\rm calc}$ [10]	$\Gamma_\alpha^{\rm calc}$	$\langle r^2\rangle_{\rm calc}$ (fm^2)
0^+	0.000	(0.621)					19.491
2^+	1.083	1.184	120 ± 37	98			19.293
4^+	2.454	2.265	277 ± 55	130			18.724
6^+	4.015	3.744	157 ± 28	122			17.783
8^+	6.509	5.500	>14	96	≪0.001	0.019	16.550
10^+	7.671	7.380	138 ± 28	63	≪0.001	$\sim 10^{-4}$	15.176
12^+	8.039	9.191	<60	30	≪0.001	1.2×10^{-3}	13.820
1^-	6.220	7.560			≪0.001	$\sim 10^{-4}$	26.689
3^-	7.340	8.507		233	≪0.001	$\sim 10^{-4}$	26.163
5^-	9.400	10.074		248	0.039	0.017	24.918
7^-	11.950	12.195		215	0.454	0.606	22.909
9^-		14.766		157	0.995	1.086	20.358
11^-		17.605		94	0.446	0.311	17.726
13^-		20.459		40	0.037	0.020	15.412

investigations have been performed to explain the α-cluster states of ^{44}Ti and their properties. Most of these calculations have satisfactorily reproduced the yrast band properties and predicted the unknown negative-parity states together with their transition probabilities as well as the α-^{40}Ca cluster-core separations to validate the α-cluster picture of the nucleus ^{44}Ti [18,19,30–32]. In fact Ref. [30] successfully considered a unified treatment of the low- and high-energy α-cluster bands within the excited-core plus α-cluster formalism.

In the present work the energy levels for both the positive- and the negative-parity bands have been satisfactorily reproduced except for the underbound 0^+ state, similar to the situation in ^{20}Ne (see Table III). The predicted 1^- and 3^- states are also seen to be approximately 1 MeV above their experimental counterparts. The agreement between the calculated and the experimental reduced $B(E2)$ transition probabilities for the positive-parity band is also good save the 4^+ and 10^+ states that are a factor of ∼2 away from the experimental values. We predict strongly enhanced probabilities for the negative-parity band which follows the expected trend and favors a core-cluster system with increasing compactness as the angular-momentum increases. In Fig. 3 we compare our results with those from previous calculations that employed the folding interactions [19] and a modified phenomenological Saxon–Wood interaction [17]. As can be seen from the figure all the theoretical calculations predict similar trends with strongly enhanced $5^- \longrightarrow 3^-$ transitions. Our results (solid line) are found generally to lie between those of the zero-range and finite-range folding interaction of Merchant *et al.* [19], thus giving us some level of confidence in our predictions. The decay widths are compared with those of Ref. [10] in the sixth and seventh columns of Table III. For the 9^-, 11^-, and 13^- states we use the predicted excitation energies to determine their respective widths. The predicted excitation energies (and decay widths) for these states, using a fixed radius of 3.96028 fm appropriate for reproducing the experimental energy for the 7^- state with the code GAMOW, are respectively 14.479 MeV (0.688 keV), 17.273 MeV (0.206 keV), and 20.102 MeV (0.02 keV). Our calculated cluster-core separation and consequently the rms charge radii are seen to decrease with increasing angular momentum. The same holds for the excited negative-parity band where we obtain larger values, consistent with the requirement of nonoverlapping cluster systems. The predicted ground-state rms charge radius of 3.590 fm compares favorably with 3.6115 ± 0.0051 fm quoted in Ref. [34]. The ratio of the cluster-core separations to the rms charge radii for ^{44}Ti is found to range from 86% for the ground state to 72% for the 12^+ state showing a similar implied α-cluster trend as for the ^{20}Ne nucleus.

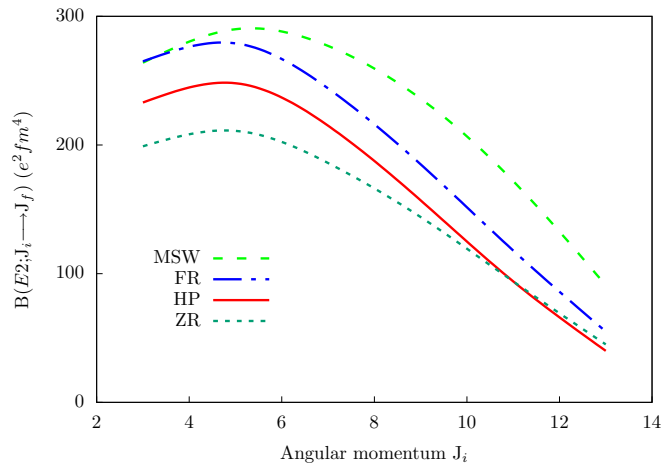

FIG. 3. Plots of the predicted $B(E2\downarrow)$ against the angular momentum using the modified Saxon-Woods interaction (MSW) [17], finite-range folding interaction (FR) [19], hybrid potential of the present work (HP), and zero-range folding interaction (ZR) [19].

TABLE IV. The measured and calculated energy levels, the reduced transition strengths $B(E2\downarrow)$, and the α-decay widths Γ_α of ^{94}Mo. The last column indicates the mean-square separation of the α-core system. The core charge radius of 4.28 ± 0.02 fm is used. Experimental data are taken from Refs. [26,36].

	Energy (MeV)		Quadrupole transition (e^2 fm^4)		Decay widths (keV)	Mean-square separation
J^π	$E_{\rm expt}$	$E_{\rm calc}$	$B(E2\downarrow)_{\rm expt}$	$B(E2\downarrow)_{\rm calc}$	$\Gamma_\alpha^{\rm calc}$	$\langle r^2\rangle_{\rm calc}$ (fm^2)
0^+	0.000	(0.484)				25.751
2^+	0.871	0.805	406 ± 10	190.0		25.589
4^+	1.574	1.387	660 ± 101	258.5		25.155
6^+	2.423	2.138		258.8	$\sim 10^{-4}$	24.461
8^+	2.956	2.967	0.124 ± 0.020	232.7	1.8×10^{-3}	23.565
10^+	3.897	3.759		191.7	1.2×10^{-3}	22.558
12^+	4.192	4.372		143.1	$\sim 10^{-4}$	21.552
14^+		4.629		92.3		20.650
16^+		4.329				19.941
1^-		1.393				27.039
3^-	2.534	1.881		266		26.733
5^-	2.611	2.610		293	3.4×10^{-3}	26.139
7^-	3.368	3.500		280	4.4×10^{-3}	25.284
9^-	4.097	4.460		244	8.0×10^{-3}	24.239
11^-	4.750	5.370		197	3.2×10^{-3}	23.108
13^-	5.734	6.082		145	1.4×10^{-3}	22.005

3. ^{94}Mo

Earlier investigation of the quasibound states and the scattering properties of the α-^{90}Zr system suggested an α-cluster structure interpretation of the yrast band of ^{94}Mo nucleus [11,23,29]. The persistency of the cluster structure in the $N = 52$ isotones, of which ^{94}Mo is a member, was discussed in Ref. [35]. These studies successfully predicted the state excitation energies and the enhanced $B(E2)$ transition probabilities currently known between the lowest states, using a global quantum number $G = 16$. Good predictions for the lowest $E2$ transitions were, in particular, given by the density-dependent double-folding interaction [29]. The experimental search for the negative-parity partners of the $K = 0^+$ band, the existence of which was predicted based on the α-cluster systematics of lighter nuclei, were not successful. The data obtained via the $(^6{\rm Li}, d)$ reaction were reported to have been contaminated with a huge background [21]. Table IV compares the calculated observables with the available corresponding data for ^{94}Mo. The energies of the 0^+, 2^+, and 4^+ states are predicted below the α-breakup threshold (2.067 MeV), in agreement with the experimental data. The shortcomings of the interaction in the interior are also evinced by the underbinding of the 0^+ ground state, as is also found in the lighter nuclei. It is, however, difficult to comment definitively on the character of the 16^+ state placed below the 12^+ state by the calculation due to our inability to predict the absolute experimental energies and the paucity of the data. We note that a similar inversion predicted for the ^{212}Po nucleus was used to explain the missing 16^+ in its ground band. This position was supported by the observed 18^+ isomeric state and its electromagnetic decay systematics [10]. In analogy with the situation in ^{212}Po however, we may posit that a similar inversion could exist in ^{94}Mo which then accounts for the unobserved 14^+ and 16^+ states, as would be expected from the model prediction and the observations in light nuclei. The calculated $B(E2)$ transition strength for ^{94}Mo is typically a factor $\sim$2–3 away from the observed values. This may be understood from the surface character of the wave function, which is not as stretched as was found in the earlier work which employs the double-folding interaction [29]. Members of the positive-parity band were also experimentally indicated to decay via magnetic octupole $M3$ as well as with electric-quadrupole $E2$ transitions. The weak measured $B(E2)$ transition strength of the 8^+ state, which may be taken as a result of the competition between the $M3$ and the two $E2$ transitions to the 6^+ states at 2.423 MeV and 2.872 MeV, disagrees with the model prediction. The rms charge radius $\langle R^2\rangle^{1/2} = 4.330$ fm obtained for the ground state is found to agree with the measured value 4.334 ± 0.016 fm listed in Ref. [26].

The systematics of the negative-parity partner bandhead in the lighter nuclei, especially in ^{20}Ne and ^{44}Ti, suggest a bandhead $\sim$1 MeV above the threshold. For ^{94}Mo, the negative-parity bandhead may thus be expected to exist a little above the α-emission threshold and possibly close to the 8^+ state. The available data, however, show a tentative negative-parity band for which we take the lowest observed 3^- state below the threshold as a band member. With the potential parameters in Table I, the negative-parity bandhead is calculated at $\sim$7 MeV which, although it agrees with earlier predictions [21,35], clearly disagrees with the observed data. This seems to suggest that members of the negative-parity partner band are yet to be found if the band exists at all, or that the α-cluster structure in the ^{94}Mo nucleus is different from that in the lighter nuclei. Adopting a parity-dependent potential such that the depth parameter V_o is increased by $\approx$7.5% ($V_o = 259.02$ MeV) so as to reproduce the 5^- quasibound state, the energies generated with the new depth are displayed in Table IV.

TABLE V. The calculated energy levels, the reduced transition strengths $B(E2\downarrow)$, and the calculated α-decay widths Γ_α of ^{104}Te. The last columns is the mean-square separation of the α-core system. Experimental data are taken from Refs. [16,34].

	Energy (MeV)		Quadrupole transition (e^2fm^4)	Decay widths (keV)	Mean-sq. separation
J^π	E_{calc}	E_{calc} [38]	$B(E2\downarrow)_{calc}$	Γ_α^{calc}	$\langle r^2\rangle_{calc}$ (fm^2)
0^+	(−0.004)	0.000		2.317×10^{-14}	27.702
2^+	0.354	0.649	223.5	1.508×10^{-13}	27.502
4^+	1.027	1.385	304.6	1.992×10^{-12}	27.002
6^+	1.926	2.211	304.9	1.627×10^{-11}	26.185
8^+	2.962	3.123	273.8	4.440×10^{-11}	25.118
10^+	4.022	4.115	224.9	2.981×10^{-11}	23.915
12^+	4.959	5.189	167.3	3.900×10^{-12}	22.717
14^+	5.588	6.377	107.6	6.875×10^{-14}	21.654
16^+	5.695	7.742	50.6	7.398×10^{-17}	20.841

Successive members of the excited negative-parity band are seen to be connected by $E2$ transitions, except for the 5^- and 3^- states, although lifetimes could not be measured, so their experimental $B(E2)$ values are not available. These negative-parity states are also observed to decay via $E1$ transitions to the positive-parity band members, except for the 9^- state. The 3^- state is connected to the 2^+ and 4^+ states via electric-dipole $E1$ transitions with observed strengths 5.062×10^{-5} W.u. and 2.1×10^{-4} W.u., respectively. Although these values are consistent with the observed very small $E1$s in heavy nuclei suggesting approximate compliance with the no-dipole condition ($\frac{Z_1}{A_1} \approx \frac{Z_2}{A_2} \approx \frac{Z}{A}$) as in earlier work [37]. The expected ratio $B(E1; J_i \to J_i + 1)/B(E1; J_i \to J_i - 1) \sim 1$, consistent also with the observations in heavy nuclei, is, however, a factor of ∼4 smaller than the observed ratio. Clearly, the cluster wave functions do not adequately account for the relative strength. This may be taken to suggest the existence of other nuclear structure effects. The calculated $B(E2\downarrow)$ values are the same order of magnitude as for the positive-parity band unlike those of the light nuclei. The decay widths are very narrow and they are also comparable to those obtained for the positive-parity band. These values are orders of magnitude smaller compared with those observed in ^{20}Ne and the predictions in ^{44}Ti. The cluster-core separations are seen to present similar magnitudes and trends for both the positive and negative-parity bands with the ground-state value being 85% of the sum of charge radii of the cluster and core nuclei.

4. ^{104}Te and ^{136}Te

The tellurium nuclei ^{104,136}Te can both be described as an α-cluster outside the doubly magic cores ^{100,132}Sn. These optimal α-core systems are expected to exhibit the signatures of α-cluster structure. However, the available experimental data, apart from the recent α-decay measurement [16], is nonexistent for ^{104}Te and do not provide any immediate information on possible α-cluster structure. Experimental searches for the location and properties of these respective α-cluster states would be highly desirable. Theoretical considerations of these α-core systems also provide further motivation for such experimental studies.

The correlation of the nucleons above the core in ^{104}Te has been shown to favor a substantial alpha-particle preformation probability somewhat larger than that obtained for ^{212}Po [16]. This was taken to suggest a superallowed character of the alpha transitions in the nuclei [16,38,39]. The α-decay energy and the half-life of the ground state as well as the possible energy structure of the nucleus have also been discussed in Refs. [38,39]. With potential parameters $R = 5.342$ MeV and $a = 0.747$ fm obtained from a M3Y surface fit for $x = 0.40$, the α-decay half-life $T_{1/2} = 19.7$ ns is deduced for the ground state of the nucleus. In obtaining this result the potential depth $V_o = 60A_2$ and the α-decay energy $E' = 5.1 \pm 0.2$ MeV [16] have been used together with a preformation factor $P = 1$. This half-life is to be compared with the recently measured value $T_{1/2} < 18$ ns [16]. The estimated result is also a factor of ∼4 from the prediction of Ref. [38] and the same order of magnitude as the expected experimental result according to the analysis of Ref. [39]. Considering that a properly renormalized depth will be slightly different from the estimated value, the agreement of the present calculation with the measured value is improved by a reduction of the potential depth by ∼1.5%. Table V contains the theoretical ground-state band properties of the nucleus. The excitation energies are compared with predictions from Ref. [38]. Both the $B(E2\downarrow)$ and the mean-separation radii are seen to present trends similar to those of other nuclei modeled as α-particle–double-closed-shell-core systems. The decay widths deduced semiclassically by using the predicted state energies show, qualitatively, the superallowed decay character of the nucleus with the 16^+ state α-decay half-life of ≈6 μs. The estimated ground-state charge radius $\langle R^2\rangle^{1/2} = 4.387$ fm is obtained by using the theoretical value 4.340 fm for the ^{100}Sn core.

For the neutron-rich isotope ^{136}Te, the protons and neutrons in the α-particle are distributed outside different shell closures, similar to the widely studied ^{212}Po nucleus. As seen in Table VI the yrast band and the observed $B(E2 : 2^+ \to 0^+)$ are satisfactorily reproduced. The calculated $B(E2\downarrow)$ for the band is also compared with calculations of Ref. [40]. We emphasize that these results are obtained without effective charge. Thus, given the predicted probabilities and the trend in the lighter nuclei modeled as α-particle–double-closed-shell-core systems discussed earlier, there is the likelihood of the excited states of ^{136}Te being characterized with equally large $B(E2\downarrow)$ values. The calculated ground-state charge radius 4.745 fm is to be compared with a measured value of

TABLE VI. The measured and calculated energy levels, the reduced transition strengths $B(E2\downarrow)$, and the calculated α-decay widths Γ_α of ^{136}Te. The last column is the mean-square separation of the α-core system. Experimental data are taken from Refs. [26,43].

	Energy (MeV)		Quadrupole transition (e^2 fm^4)			Decay widths (keV)	Mean-sq. sep.
J^π	$E_{\rm expt}$	$E_{\rm calc}$	$B(E2\downarrow)_{\rm expt}$	$B(E2\downarrow)_{\rm calc}$	$B(E2\downarrow)_{\rm calc}$ [40]	$\Gamma_\alpha^{\rm calc}$	$\langle r^2\rangle_{\rm calc}$ (fm^2)
0^+	0.000	(0.180)					29.298
2^+	0.607	0.435	206 ± 30	251.5	286.6	6×10^{-4}	29.148
4^+	1.030	0.896		345.9	399.4		28.757
6^+	1.383	1.490		353.2	416.1		28.137
8^+	2.132	2.150		328.5	396.9	8×10^{-4}	27.335
10^+	2.792	2.794		285.4	355.5	1.6×10^{-3}	26.425
12^+	3.187	3.320		231.4	298.8		25.500
14^+	3.720	3.600		172.1	232.2	8×10^{-4}	25.655
16^+		3.480					23.983
18^+		3.380					23.575
1^-		6.884					35.067
3^-		7.313		457.7			34.634
5^-		7.977		507.8			33.789
7^-		8.816		487.9			32.576
9^-		9.757		433.7			31.099
11^-		10.702		360.8			29.504

4.7815 ± 0.0089 fm [34]. Both the magnitude of the calculated decay width and the trend of the mean cluster-core separation are the same as for the ^{44}Ti nucleus. Measurement of these properties is expected to provide the evidence needed to confirm the cluster structure in this nucleus. The negative-parity bandhead is placed at ~6.6 MeV above the threshold. The negative-parity states and the corresponding transitions will hopefully guide further experimental investigations of the nucleus, for example, from angle correlation measurements with the (^{7}Li, $t\alpha$) reaction.

5. General comments on the potential

As seen from our calculations, the 0^+ ground state is consistently underbound for all the nuclei. The same holds for calculations of exotic cluster structure of heavier nuclei. The underbinding of the 0^+ state may be corrected by introducing a short-range interaction of the form $V_\delta(r) = -V_1$ for $r \leqslant r_o$ and $V_\delta(r) = 0$ for $r > r_o$, where the range $r_o \approx \frac{1}{2}[r_1(0) + r_1(2)]$ is taken as the average of the first turning points $r_1(0)$ and $r_1(2)$ for the 0^+ and 2^+ states, respectively [41,42]. The interaction is observed to lower the $r_1(0)$ turning point and consequently the 0^+ state. The initial poor estimate of the first turning point $r_1(0)$ and hence the failure of the (SW + SW^3) potential may then be due to the possible existence of the core-cluster overlap in the region close to $r \sim 0$. Thus the range r_o may be taken to correspond to the width of the nucleon distribution in the overlap region. For the nuclei studied here, the depth V_1 is seen to depend on the degree of underbinding, and the values of r_o are nearly constant for all the α-particle–double-closed-shell-core systems examined, with an average value of 0.283 fm, in agreement with our previous estimate for ^{212}Po = ^{208}Pb $\otimes\, \alpha$ [41]. This is demonstrated by plotting r_o against the core mass numbers A_1 (Fig. 4). The actual values are seen to decrease with increasing mass, indicating that the α-core overlapping densities are largest for the lighter nuclei.

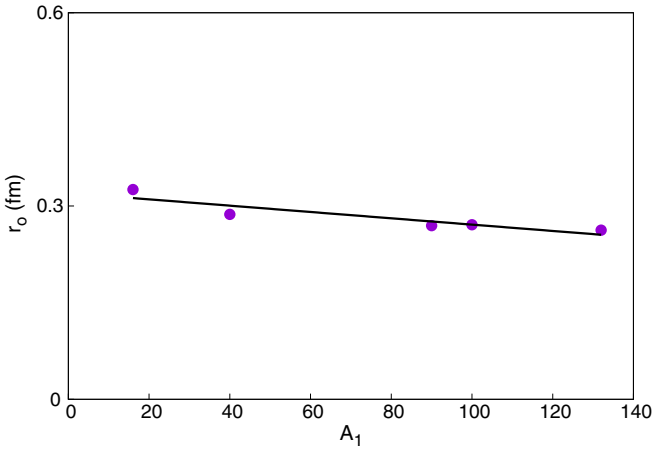

FIG. 4. Plot of the interaction range r_o (fm) against the core mass A_1.

IV. CONCLUSIONS

We have developed a local potential cluster model with a cluster-core nuclear potential parametrized in the Saxon-Woods (SW + SW^3) form, to improve on previous usage by taking the strength, radius, diffuseness and mixing parameter from the double-folding M3Y potential model. With it we have calculated spectra, reduced electromagnetic $B(E2)$ transition strengths, mean-square charge radii, and, where appropriate, α-decay widths for the ground-state $K^\pi = 0^+$ and first-excited $K^\pi = 0^-$ bands of ^{20}Ne, ^{44}Ti, ^{94}Mo, ^{104}Te, and ^{136}Te. These nuclei can all be modeled as α-particle–double-closed-shell-core systems and as such are expected to be the best candidates to show pronounced α-cluster structure.

The lightest two of these nuclei, ^{20}Ne and ^{44}Ti, have been thoroughly investigated experimentally so that among the quantities we calculate, only the lifetimes of the excited

negative-parity band in ^{44}Ti, leading to $B(E2)$ values, remain to be measured. These nuclei are firmly established as displaying α-clustering and our calculations (without any effective charges) are in good agreement with both the available data and with many other theoretical calculations.

The nucleus ^{94}Mo is generally considered to display α-clustering as well, but there are significant gaps in the experimental data available for it. Only a few lifetimes have been measured to deduce $B(E2)$ values for comparison against our predictions, and there are no available experimental α-decay widths at all. Thus our calculations for these latter quantities are purely predictive and suggest that measurements of the decay widths will be quite challenging for experimentalists in view of the smallness (typically ∼eV) of the expected values. Nevertheless, measurement of these quantities is essential to provide thoroughly convincing confirmation of the α-cluster nature of these states.

Our calculations for ^{104}Te and ^{136}Te are original within this model. At the moment the only experimental data to compare against are energy levels and a single measured $B(E2)$ value in ^{136}Te. Since these two nuclei are both so far outside the valley of β stability, and indeed rather close to the proton and neutron driplines, respectively, it will be very interesting to see if future experiments can confirm that they are truly good α-cluster nuclei and that the same models that have been successful for lighter nuclei continue to work in this region.

Note added. Before this work could be completed, one of the authors, Sandro M. Perez, passed away.

[1] M. Freer, Rep. Prog. Phys. **70**, 2149 (2007).
[2] D. M. Brink, J. Phys.: Conf. Ser. **111**, 012001 (2008).
[3] H. Horiuch, J. Phys.: Conf. Ser. **569**, 012001 (2014).
[4] M. Freer and A. C. Merchant, J. Phys. G **23**, 261 (1997).
[5] H. Matsuno, N. Itagaki, T. Ichikawa, Y. Yoshida, and Y. Kanada-En'yo, Prog. Theor. Exp. Phys. 063D01 (2017).
[6] V. Z. Gol'dberg, V. P. Rudakov, and V. A. Timofeev, Sov. J. Nucl. Phys. **19**, 253 (1974).
[7] T. Yamada and Y. Funaki, Phys. Rev. C **92**, 034326 (2015).
[8] A. Volya and Yu. M. Tchuvil'sky, Phys. At. Nucl. **79**, 772 (2016).
[9] B. Buck, A. C. Dover, and J. P. Vary, Phys. Rev. C **11**, 1803 (1975).
[10] B. Buck, J. C. Johnston, A. C. Merchant, and S. M. Perez, Phys. Rev. C **53**, 2841 (1996).
[11] F. Michel, G. Reidemeister, and S. Ohkubo, Phys. Rev. C **61**, 041601(R) (2000).
[12] T. T. Ibrahim, S. M. Perez, and S. M. Wyngaardt, Phys. Rev. C **82**, 034302 (2010).
[13] T. T. Ibrahim, S. M. Perez, S. M. Wyngaardt, B. Buck, and A. C. Merchant, Phys. Rev. C **85**, 044313 (2012).
[14] D. K. Nauruzbayev, V. Z. Goldberg, A. K. Nurmukhanbetova, M. S. Golovkov, A. Volya, G. V. Rogachev, and R. E. Tribble, Phys. Rev. C **96**, 014322 (2017).
[15] M. Fukada, M. K. Takimoto, K. Ogino, and S. Ohkubo, Phys. Rev. C **80**, 064613 (2009).
[16] K. Auranen, D. Seweryniak, M. Albers, A. D. Ayangeakaa, S. Bottoni, M. P. Carpenter, C. J. Chiara, P. Copp, H. M. David, D. T. Doherty, J. Harker, C. R. Hoffman, R. V. F. Janssens, T. L. Khoo, S. A. Kuvin, T. Lauritsen, G. Lotay, A. M. Rogers, J. Sethi, C. Scholey, R. Talwar, W. B. Walters, P. J. Woods, and S. Zhu, Phys. Rev. Lett. **121**, 182501 (2018).
[17] F. Michel, G. Reidemeister, and S. Ohkubo, Phys. Rev. Lett. **57**, 1215 (1986); Phys. Rev. C **37**, 292 (1988).
[18] S. Ohkubo, Phys. Rev. C **38**, 2377 (1988).
[19] A. C. Merchant, K. F. Pal, and P. E. Hodgson, J. Phys. G **15**, 601 (1989).
[20] T. Yamaya, S. Oh-ami, M. Fujiwara, T. Itahashi, K. Katori, M. Tosaki, S. Kato, S. Hatori, and S. Ohkubo, Phys. Rev. C **42**, 1935 (1990).
[21] T. Yamaya, K. Ishigaki, H. Ishiyama, T. Suehiro, S. Kato, M. Fujiwara, K. Katori, M. H. Tanaka, S. Kubono, V. Guimaraes, and S. Ohkubo, Phys. Rev. C **53**, 131 (1996); T. Yamaya, K. Katori, M. Fujiwara, S. Kato, and S. Ohkubo, Prog. Theor. Phys. Suppl. **132**, 73 (1998).
[22] P. Guazzoni, M. Jaskola, L. Zetta, C. Y. Kim, T. Udagawa, and G. Bohlen, Nucl. Phys. A **564**, 425 (1993).
[23] B. Buck, A. C. Merchant, and S. M. Perez, Phys. Rev. C **51**, 559 (1995).
[24] B. Buck, A. C. Merchant, and S. M. Perez, Phys. Rev. Lett. **76**, 380 (1996).
[25] B. Buck, A. C. Merchant, and S. M. Perez, Nucl. Phys. A **617**, 195 (1997); **625**, 554 (1997); Phys. Rev. C **58**, 2049 (1998).
[26] H. De Vries, C. W. De Jager, and C. De Vries, At. Data Nucl. Data Tables **36**, 495 (1987).
[27] T. Vertse, K. F. Pal, and Z. Balogh, Comput. Phys. Commun. **27**, 309 (1982).
[28] D. Ni and Z. Ren, Phys. Rev. C **83**, 014310 (2011).
[29] S. Ohkubo, Phys. Rev. Lett. **74**, 2176 (1995).
[30] S. Ohkubo, Y. Hirabayashi, and T. Sakuda, Phys. Rev. C **57**, 2760 (1998).
[31] J. Zhang, W. D. M. Rae, and A. C. Merchant, Phys. Rev. C **53**, 515 (1996).
[32] F. Koyuncu, A. Soylu, and O. Bayrak, Mod. Phys. Lett. A **32**, 1750050 (2017).
[33] J. Chen, B. Singh, and J. A. Cameron, Nucl. Data Sheets **112**, 2357 (2011).
[34] I. Angeli and K. P. Marinova, At. Data Nucl. Data Tables **99**, 69 (2013).
[35] M. A. Souza and H. Miyake, Phys. Rev. C **91**, 034320 (2015).
[36] D. Abriola and A. A. Sonzogni, Nucl. Data Sheets **107**, 2423 (2006).
[37] B. Buck, A. C. Merchant, M. J. Horner, and S. M. Perez, Phys. Rev. C **61**, 024314 (2000).
[38] P. Mohr, Eur. Phys. J. A **31**, 23 (2007).
[39] M. Patial, R. J. Liotta, and R. Wyss, Phys. Rev. C **93**, 054326 (2016).
[40] S. M. Wang, J. C. Pei, and F. R. Xu, Phys. Rev. C **87**, 014311 (2013).
[41] T. T. Ibrahim, S. M. Wyngaardt, and B. D. C. Kimene Kaya, Nucl. Phys. A **966**, 73 (2017).
[42] B. D. C. Kimene Kaya, S. M. Wyngaardt, T. T. Ibrahim, and W. A Yahya, Phys. Rev. C **98**, 044308 (2018).
[43] A. A. Sonzogni, Nucl. Data Sheets **95**, 837 (2002).